Application of a dynamic subgrid-scale model to turbulent recirculating flows

By Y. Zang[1], R. L. Street[1] AND J. R. Koseff[1]

The dynamic subgrid-scale model of Germano *et al.* (1991) is implemented in a finite volume formulation and applied to the simulation of turbulent flow in a three-dimensional lid-driven cavity at Reynolds number of 7500. The filtering operation is carried out in physical space, and the model coefficient is calculated locally. The computed mean and r.m.s. velocities as well as the Reynolds stress are compared with experimental data. It is shown that backscatter from small to large scales is necessary to sustain turbulent fluctuations. The model is being applied to the simulation of turbulent flows in stratified and rotating environment in complex geometries.

1. Motivations and objectives

Simulation of most engineering, environmental, or geophysical flows requires the use of turbulence model to represent unresolved small scale motions. Large eddy simulation (LES), which computes the motion of large spatial scales explicitly and models that of subgrid scales, proves to be an effective tool. During the last three decades, extensive effort has been put into developing subgrid-scale (SGS) turbulence models. Conventional SGS models such as the popular Smagorinsky (1963) model have several significant drawbacks. For example, they usually require model constants as input. These constants are not universal and have to be optimized to fit each type of flow. Although the Smagorinsky model has been successfully used in both homogeneous and wall-bounded turbulent flows (Bardina *et al.* 1983; Piomelli *et al.* 1988), it was found to be too dissipative in wall-bounded transitional flows (Piomelli *et al.* 1990), partly because the model does not account for the effect of energy backscatter from small to large scales. In addition, the Smagorinsky model gives a non-zero SGS stress in laminar flows.

Recently, Germano *et al.* (1991) developed a new SGS model which calculates the model coefficient dynamically using the smallest resolved scales. This dynamic SGS model (hereafter referred to as DSM) has many desirable features such as requiring only one input parameter, exhibiting the correct asymptotic behavior near solid walls and in laminar flow, and being capable of accounting for energy backscatter. Most of the studies so far using the dynamic model has coupled it with spectral methods and computed flows with one or more homogeneous directions (Germano *et. al.* 1991; Moin *et. al.* 1991).

The long-term goal of this project is to develop a numerical model to investigate environmental or geophysical flows in complex geometries. These flows are highly

1 Stanford University

inhomogeneous and may contain local regions of laminar, transitional, or turbulent flows of which successful simulations require a SGS model that can adjust itself to local flow dynamics – a quality which DSM possesses. The immediate objectives of the present work are to incorporate DSM into a finite volume Navier-Stokes code (Zang *et. al.* 1992) which is written in the general curvilinear coordinate system and to examine the model's applicability to turbulent recirculating flows. We performed large eddy simulations of flow in a lid-driven cavity at a Reynolds number of 7500. The computed mean and fluctuating profiles were compared with experimental data. Local averaging of the model coefficient was investigated. The model is being applied to the simulation of stratified rotating upwelling flows on a slopping bottom.

2. Accomplishments

2.1. The finite-volume implementation of DSM

The SGS Reynolds stress after applying the grid filtering operation represented by an overbar to the momentum equation is

$$\tau_{ij} = \overline{u_i u_j} - \overline{u}_i \overline{u}_j \tag{1}$$

The Smagorinsky model is employed as the base model for τ_{ij} as

$$\tau_{ij} - \frac{\delta_{ij}}{3}\tau_{kk} = -2\nu_T \overline{S}_{ij} \tag{2}$$

where the eddy viscosity

$$\nu_T = C\overline{\Delta}^2 |\overline{S}| \tag{3}$$

$\overline{\Delta}$ is the grid filter width, $|\overline{S}| = (2\overline{S}_{ij}\overline{S}_{ij})^{1/2}$ is the magnitude of the resolved large-scale strain rate tensor

$$\overline{S}_{ij} = \frac{1}{2}\left(\frac{\partial \overline{u}_i}{\partial x_j} + \frac{\partial \overline{u}_j}{\partial x_i}\right) \tag{4}$$

and C is the model coefficient which is to be computed dynamically using the procedure described below. We note that C is the square of the commonly used Smagorinsky constant C_S.

Following Germano *et al.* (1991), we introduce a test-scale filter represented by a tilde whose length scale $\widetilde{\overline{\Delta}}$ is larger than $\overline{\Delta}$. The purpose of doing this is to utilize the information between the grid-scale and the test-scale filters to determine the characteristics of the SGS motion. By applying Germano's algebraic identity (Germano 1991) relating the subgrid-scale stress and the test-scale stress and employing a least-square closure (Lilly 1992), we obtain an explicit expression for the model coefficient C based on the local flowfield as

$$C = -\frac{\mathcal{L}_{ij} M_{ij}}{2\overline{\Delta}^2 M_{ij} M_{ij}} \tag{5}$$

where

$$\mathcal{L}_{ij} = \widetilde{\overline{u}_i \overline{u}_j} - \widetilde{\overline{u}}_i \widetilde{\overline{u}}_j, \tag{6a}$$

$$M_{ij} = \alpha^2 |\widetilde{\overline{S}}| \widetilde{\overline{S}}_{ij} - \widetilde{|\overline{S}| \overline{S}_{ij}}, \tag{6b}$$

$$\alpha = \widetilde{\Delta}/\Delta. \tag{6c}$$

In the above model, α is the only input parameter.

The implementation of the SGS stress term '$-\partial \tau_{ij}/\partial x_j$' in the momentum equations needs some consideration. First the trace of τ_{ij} is combined with the pressure gradient. Then, if the time marching scheme is explicit, τ_{ij} can be calculated directly from equations (2), (3) and (4). However, if an implicit or semi-implicit time marching scheme is used, it is advantageous to advance the SGS stress term (or at least a part of it) implicitly. This requires us to express SGS stress term in terms of of the velocity as

$$-\frac{\partial \tau_{ij}}{\partial x_j} = \frac{\partial}{\partial x_j}(\nu_T \frac{\partial \overline{u}_i}{\partial x_j}) + \frac{\partial \nu_T}{\partial x_j} \frac{\partial \overline{u}_j}{\partial x_i} \tag{7}$$

In deriving the above equation, we have utilized the continuity equation. The first term on the right-hand-side of equation (7) can be combined with the viscous terms and be advanced in time implicitly. The second term, on the other hand, poses difficulty if treated implicitly because by doing so, the three momentum equations are coupled and the resulting matrix is more complicated. In the present work, this term is advanced explicitly as an extra source term. Numerical experiments showed that this treatment did not affect stability in the present case.

The governing equations are transformed into the computational space and discretized on a non-staggered grid using a finite volume approach (Zang *et al.* 1992). Cartesian velocity and volume fluxes are used as dependent variables. The solution method integrates the governing equations in time semi-implicitly by solving the viscous terms with the approximate factorization technique. The pressure Poisson equation is solved using a multigrid method. The overall accuracy is second-order in both space and time. The use of the non-staggered grid layout and Cartesian velocities as dependent variables makes the filtering operations very easy to carry out when the dynamic eddy viscosity is computed.

Most studies to date using DSM have carried out filter operations in wave space. Recently, effort has been made to evaluate the behavior of different kinds of filters in physical space (Lund 1991). In the present formulation, we employ a top-hat filter in physical space with the trapezoidal rule for the test-scale filter. Because of the non-staggered-grid layout, all the variables that are used in the calculation of C are defined at the center of a control volume, and thus the filtering operation is the same for every variable. The length scale of the test filter is twice of that of the grid cell resulting in an α of 2. This value of α has been shown to be the optimal choice in the simulation of a turbulent channel flow (Germano *et al.* 1991).

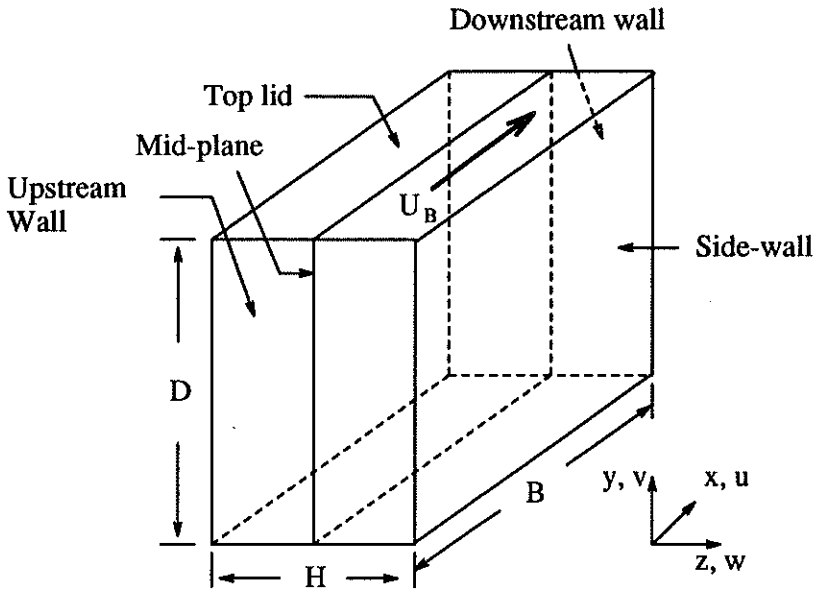

FIGURE 1. Geometry and boundary condition of the lid-driven cavity flow.

After the model coefficient C is computed from equation (4), it is averaged locally in space using the same scheme as that of the test filtering.

When local averaging of C alone was employed, numerical instability was experienced. This occurred because a large and negative C could lead to a negative eddy viscosity ν_T with a magnitude larger than the molecular viscosity, resulting in a negative total viscosity. Similar instability has been observed in previous simulations using the dynamic model and a local model coefficient $C(x, y, z, t)$ (Cabot 1991). When there are one or more homogeneous directions, a plane or line average in those directions could be used to stabilize the calculation (e.g., Germano *et al.* 1991). In the present wall-bounded flows, however, there is no homogeneous direction. Larger averaging volume and/or averaging in time could be employed to reduce the magnitude of negative Cs (Piomelli 1991), but they still do not generally guarantee stability. To overcome this difficulty, we set the total viscosity $\nu_T + \nu$ equal to zero wherever it becomes negative. This cutoff eliminates the negative total viscosity that causes the numerical instability and at the same time allows energy to backscatter from small to large scales. The local averaging before the cutoff serves to spread the effect of large negative values of C if they exist. For the case computed in this work, the cutoff does not affect the flow significantly as the magnitude of the negative ν_T is larger than ν only in a very localized region near the upper right corner of the cavity.

2.2. LES of flow in a lid-driven cavity

Lid-driven laminar flows in a cavity have long been used as a benchmark to test the accuracy of numerical methods (e.g., Ghia *et al.* 1982; Perng & Street

1989). Although extensive experimental measurements have been performed for transitional and turbulent flows in cavities (Koseff & Street 1984; Prasad & Koseff 1989), to the authors' knowledge, there have been no detailed direct or large-eddy simulations. Part of the difficulty lies in that in its temporal evolution the flow goes through the whole range of laminar, transitional, and turbulent stages. Moreover, even at the fully developed state, the flow is highly inhomogeneous and may have both laminar and turbulent regions. Successful simulation of this flow requires a SGS model which is capable of adjusting itself to the local flow dynamics.

We computed the lid-driven flow in a three-dimensional cavity with aspect ratios B:D:H of 1:1:0.5. A schematic of the cavity together with the notations are given in Figure 1. The Reynolds number based on the lid velocity U_B and the cavity length B is 7500. Past experiments (Koseff & Street 1984) have shown that at Reynolds numbers higher than about 6000, instabilities occur near the downstream eddy. As the Reynolds number increases, the flow becomes increasingly turbulent near walls, and at Reynolds numbers higher than 10,000, the flow near downstream eddy becomes fully turbulent. Thus, the present flow is in the transitional regime. In the simulation, we use a 64x64x32 grid, which is non-uniform in the streamwise and vertical directions but is spanwise uniform. Initially the fluid is at rest. Computation was first carried out in a half of the cavity with a 64x64x18 grid. A symmetry boundary condition was specified at the mid-plane. After the flow was fully developed, the half flowfield was mirrored onto the whole cavity. Simulation then continued and statistics were collected after a relaxation time of three turnaround time-scale T_a of the cavity. The value of T_a, which was about 1 minute in this case, was estimated as the time for a particle at the edge of the top boundary layer to travel back to its starting position in the cavity.

Figure 2 shows the computed mean center-line velocity profiles on the mid-plane. Measurements by Prasad and Koseff (1989) are also shown. The computed statistics were collected during a period of $5T_a$, while the experimental data was averaged over periods of $5T_a$ to $10T_a$. The computation slightly over-predicts the thickness of the boundary layer on the upstream wall but captures the thickness of the bottom boundary layer and the magnitude of the two peak velocities fairly accurately. The averaged relative error between the two data sets scaled by the lid velocity is less than 2 percent.

The r.m.s. of fluctuating velocities $\sqrt{< u'^2 >}/U_B$ and $\sqrt{< v'^2 >}/U_B$ and the Reynolds stress $< u'v' > /U_B^2$ on the center-lines in the mid-plane are shown in Figure 3, where $< \cdot >$ denotes time averaging. We note that in the figure, these two quantities are increased by a scale of 10 and 500, respectively. The computation slightly over-predicts the r.m.s. of u' near the bottom boundary layer and under-predicts the r.m.s. of v' near the upstream wall. There is a minimum in the r.m.s. profile of u velocity in the bottom boundary layer which is not evident in the experimental data. The magnitude of the Reynolds stresses near the bottom and the upstream boundary layers is well represented. A maximum of the Reynolds stress is observed above the bottom boundary layer which is not shown in the experimental profile.

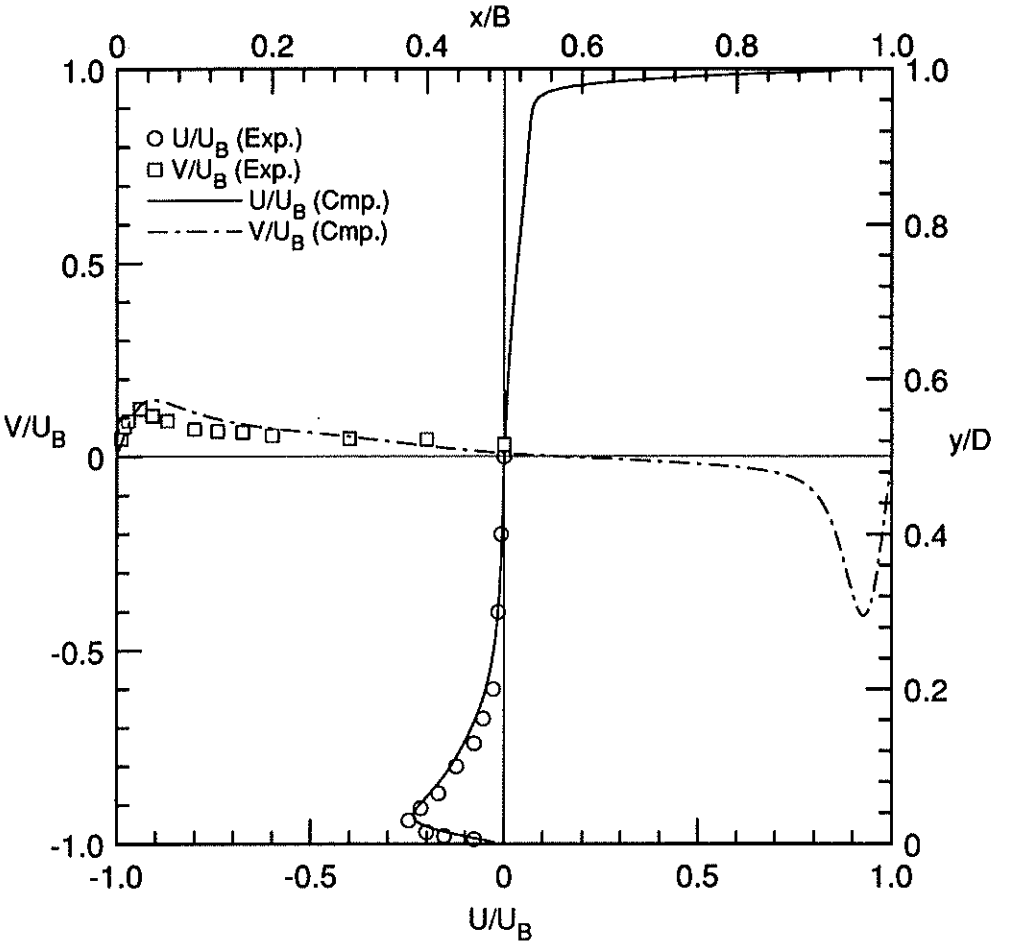

FIGURE 2. Mean centerline velocities on the mid-plane. Symbols are from Prasad and Koseff (1989). Lines are from the present computation.

The computed profiles in Figures 2 and 3 are the large-scale quantities resolved by the grid, while the experimental data contains contribution from both the large and small scales. The contribution of the SGS motion to the Reynolds stress $< u'v' >$ can be estimated using the time average of the SGS stress, $< \tau_{12} >$. In the present case, the value of $< \tau_{12} >$ is at least an order of magnitude smaller than $< \overline{u}'\overline{v}' >$ which is the large-scale contribution to the Reynolds stress. This indicates that the time-averaged statistics are well represented by the large-scale quantities. Two factors besides modeling error could have contributed to the above discrepancies. One is the experimental uncertainty, and the other is the effect of numerical resolution. However, at the present time, collecting statistics on a grid substantially finer than the one presently used is prohibitively expensive.

Figure 4a shows the dynamically computed C on the mid-plane of the cavity, and 4b displays C on a plane close to one of the side-walls. On the mid-plane,

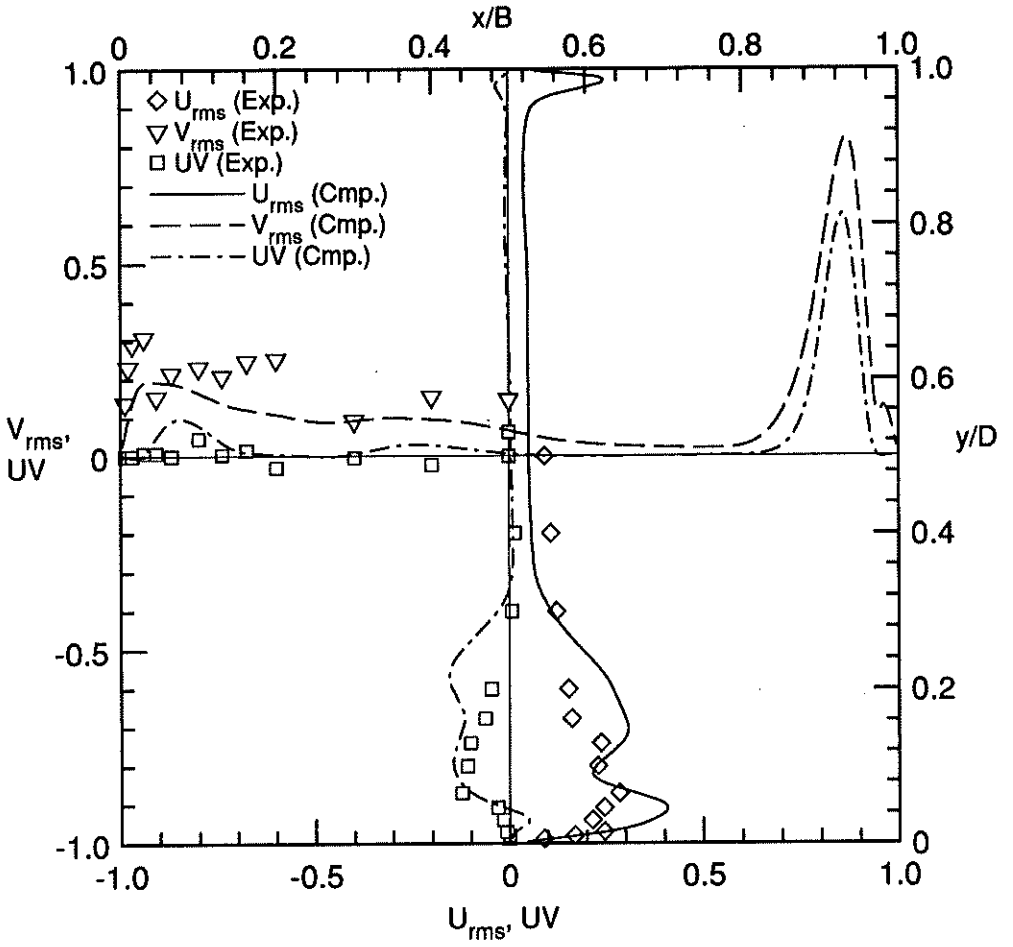

FIGURE 3. R.m.s. velocity and Reynolds stress at the centerlines on the mid-plane. $U_{rms} = 10\sqrt{< u'^2 >}/U_B$, $V_{rms} = 10\sqrt{< v'^2 >}/U_B$, $UV = 500 < u'v' > /U_B^2$. Symbols are from Prasad and Koseff (1989). Lines are from the present computation.

the range of C is from -0.12 to 0.1, while on the near-wall plane, the range is from -0.17 to 0.22. In the bulk region of the mid-plane, the magnitude of C is from 0.01 to 0.02, which is comparable to the square of the commonly used value of 0.1 for the Smagorinsky constant. On the other hand, near the side wall (Figure 4b), C is small except near the corners and in the corner boundary layers. This is consistent with the expected behavior of C near a solid wall. It is interesting to notice that C is small near the moving top lid in both planes.

There are localized regions in Figure 4 where C is negative, which results in negative eddy viscosity representing energy backscatter from small to large scales. The ability of the present model to backscatter energy to large scales is important in sustaining turbulent fluctuations in the simulation. The time history of the

FIGURE 4A. Contours of computed C on the mid-plane. Dotted lines represent negative values.

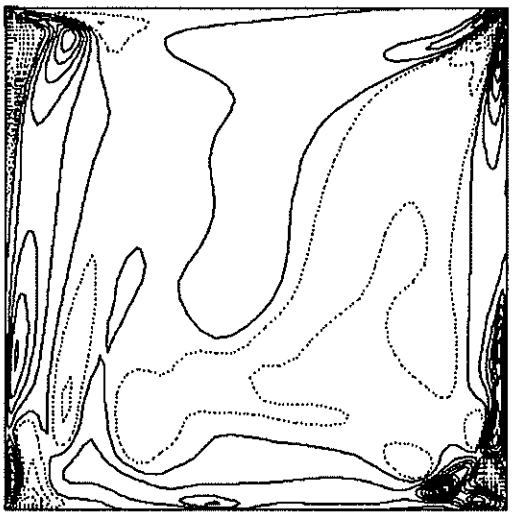

FIGURE 4B. Contours of computed C near one of the side walls. Dotted lines represent negative values.

large-scale streamwise velocity $\overline{u}(t)$ near the peak of the bottom boundary layer on the center-line of the mid-plane is shown in Figure 5a, where the flow was in its fully developed state. Figure 5b gives $\overline{u}(t)$ at the same location when no negative ν_T was allowed. The fluctuations in 5b were slowly damped out, indicating that backscatter from small to large scales is necessary to sustain turbulence. The low frequency oscillations with a period of about 1 minute in Figure 5a correspond

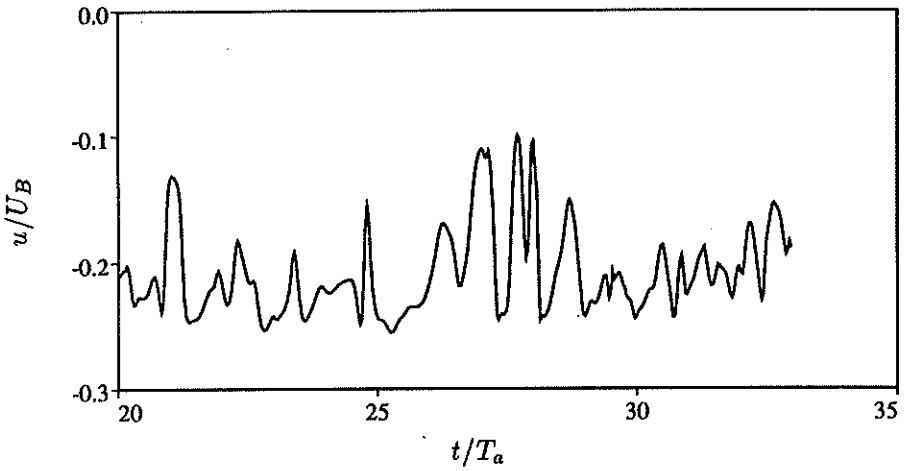

FIGURE 5A. Time history of u near the peak of the lower boundary layer on the vertical center-line in the mid-plane. Model with backscatter. Fully developed state.

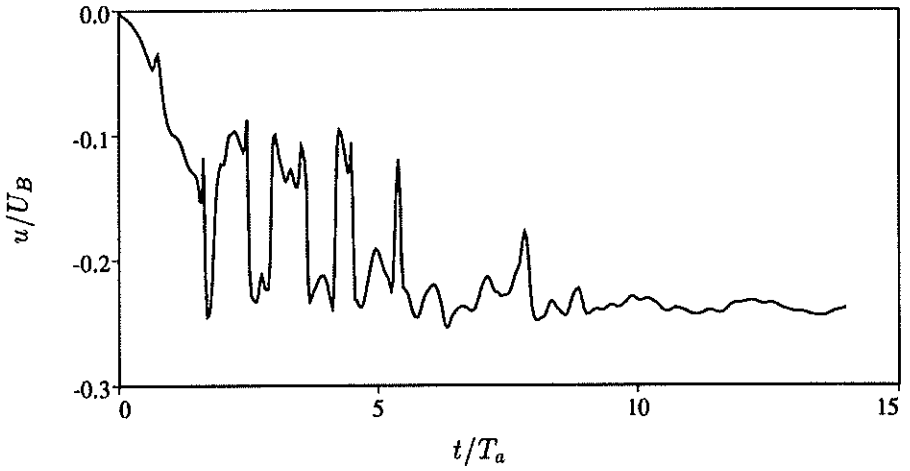

FIGURE 5B. Same as Figure 5a. Model without backscatter.

to the spanwise meandering of TGL vortices. Examination of the flow structures in the spanwise direction shows the appearance of one pair of TGL vortices near the downstream wall which is meandering spanwisely. This is consistent with past experimental results (Prasad 1989).

Previous simulations of cavity flows at lower Reynolds numbers have shown that the flows are essentially symmetric over the mid-plane (Perng & Street 1989). This is true when the flow is laminar since there is no non-symmetric forcing and any non-symmetric small disturbances are damped. However, in turbulent flows, small disturbances could be amplified and result in asymmetry. In the present case, it

was found that when the half-cavity domain was used and the symmetry boundary condition was imposed at the mid-plane, both the streamwise fluctuating velocity $< u'^2 >$ and the streamwise-vertical Reynolds stress $< u'v' >$ were unphysically large. On the other hand, the mean velocity profiles were barely changed. This was because the symmetry boundary condition eliminated the spanwise fluctuating velocity w' at the mid-plane and restricted the meandering of the TGL vortices which were responsible for the momentum and energy transfer in the spanwise direction near the mid-plane. These high frequency fluctuations are averaged out in the mean profiles but make significant contribution to the r.m.s. quantities and Reynolds stress.

3. Summaries and future plans

A dynamic SGS model is coupled with a finite volume solution method and employed in the large eddy simulation of turbulent flow in a lid-driven cavity. Local averaging together with a cutoff is employed to obtain the model coefficient. The mean and fluctuating quantities were compared with experimental data and good agreement was achieved. It was shown that backscatter is necessary to sustain fluctuations in the flow.

The model is being applied to the simulation of upwelling flows of a stratified rotating fluid on a slopping bottom. Baroclinic instability was observed at the surface density front and intensive mixing occurred on both sides of the front. Preliminary results have shown that the computed wave speed and wave size compare favorably with the experimental and theoretical values. The characteristics of the instabilities and the subsequent breakdown of the front are being investigated. The model is also being employed to investigate flows in more complex geometries.

Acknowledgement

The authors wish to thank Prof. J. H. Ferziger and Dr. T. S. Lund for many helpful suggestions. The Cray YMP allocation provided by NCAR Scientific Computing Division is gratefully appreciated. This research is supported by National Science Foundation through Grant CTS-8719509. T. Lin, who was supported by Center for Turbulence Research, made a significant contribution in the early stages of this work.

REFERENCES

BARDINA, J., FERZIGER, J. H., & REYNOLDS W. C. 1983 Improved turbulence models based on large eddy simulation of homogeneous, incompressible, turbulent flows. *Report No. TF-19.* Dept. Mech. Eng., Stanford University.

CABOT, W. 1991 Large eddy simulation of passive and buoyant scalars with dynamic subgrid-scale models. *Annual Research Briefs.* Center for Turbulence Research, Stanford U./NASA-Ames, 191-205.

GERMANO, M. 1991 Turbulence: the filtering approach. *J. Fluid Mech.* **238,** 325-336.

GERMANO, M., PIOMELLI, U., MOIN, P. & CABOT, W.H. 1991 A dynamic subgrid-scale eddy viscosity model. *Phys. Fluids A.* **3,** 1760-1765.

GHIA, U., GHIA, K. N. & SHIN, C. T. 1982 High-Re solutions for incompressible flow using the Navier-Stokes equations and a multigrid method. *J. Comp. Physics.* **48,** 387-411.

KOSEFF, J. R. & STREET, R. L. 1984 Visualization studies of a shear driven three-dimensional recirculating flow. *J. Fluids Eng.* **106,** 21-29.

LILLY, D. K. 1992 A proposed modification of the Germano subgrid scale closure method. *Phys. Fluids A.* **4,** 633-635.

LUND, T. S. 1991 Discrete filters for finite differenced large eddy simulation. Presentation at the 44th Annual Meeting of the American Physical Society, Division of Fluid Dynamics, Scottsdale, Arizona.

MOIN, P., SQUIRES, K., CABOT W. & LEE, S. 1991 A dynamic subgrid-scale model for compressible turbulence and scalar transport. *Phys. Fluids A.* **3,** 2746-2757.

PERNG, C. Y. & STREET, R. L. 1989 3-D unsteady flow simulation: alternative strategies for a volume-averaged calculation. *Int. J. Num. Meth. Fluids.* **9,** 341-362.

PIOMELLI, U. 1991 Local averaging of the dynamic subgrid-scale stress model. Presentation at the 44th Annual Meeting of the American Physical Society, Division of Fluid Dynamics, Scottsdale, Arizona.

PIOMELLI, U., MOIN, P. & FERZIGER, J. H. 1988 Model consistency in large eddy simulation of turbulent channel flows. *Phys. Fluids.* **31,** 1884-1891.

PIOMELLI, U., ZANG, T. A., SPEZIALE C. G. & HUSSAINI, M. Y. 1990 On the large-eddy simulation of transitional wall-bounded flows. *Phys. Fluids A.* **2,** 257-265.

PRASAD, A. K. 1989 Effects of variable geometry on momentum and heat transfer in a lid-driven cavity flow. Ph.D Dissertation, Dept. Mech. Eng., Stanford University.

PRASAD, A. K. & KOSEFF, J. R. 1989 Reynolds number and end-wall effects on a lid-driven cavity flow. *Phys. Fluids A.* **1,** 208-218.

SMAGORINSKY, J. 1963 General circulation experiments with the primitive equations. I. The basic experiment. *Mon. Weather Rev.* **91,** 99-164.

ZANG, Y., STREET, R. L. & KOSEFF, J. R. 1992 A non-staggered grid fractional step method for time-dependent incompressible Navier-Stokes equations in general curvilinear coordinate systems *submitted to J. Comp. Physics.*